Properties and Effects of Measurement Errors on 2D Resistivity Imaging Surveying

Zhou, Bing; Dahlin, Torleif

Published in:
Near Surface Geophysics

2003

Near Surface Geophysics, 2003, 105-117

Properties and effects of measurement errors on 2D resistivity imaging surveying

Bing Zhou[1*] and Torleif Dahlin[2]

[1] *Department of Geology and Geophysics School of Earth and Environmental Sciences, Adelaide University, South Australia 5005, Australia*

[2] *Department of Engineering Geology Lund University Box 118 S-221 00 Lund, Sweden*

Received January 2002, revision accepted June 2003

ABSTRACT

Electrode spacing errors and errors correlated with the magnitude of the observed potential are two key factors that affect the data quality for DC resistivity imaging measurements. This paper investigates the properties and effects of these two kinds of error on 2D resistivity imaging or inversion for practical applications. By analytic analysis and numerical simulations, the off-line and in-line electrode spacing errors were quantitatively estimated for all common electrode arrays (pole-pole, pole-dipole, pole-bipole, Wenner, Schlumberger, dipole-dipole, γ-array, Wenner-β) in 2D resistivity imaging surveys. Meanwhile, the spreading patterns of the spacing errors in the pseudosection and the possible artefacts in the imaging (inverted model) are evaluated. We show that the magnitude of the spacing errors are quite different with these arrays, being largest for dipole-dipole, Wenner-β and γ-array surveys, for which a 10% in-line spacing error may cause twice as large an error (>20%) in the observed resistance or apparent resistivity, which in turn will produce some artefacts in the inverted model. The observed potential errors obtained with the reciprocity principle and collected from different sites and with different electrode arrays, were analysed to show the properties of the potential error caused by many aspects in the field. Using logarithmic plots and error pseudosections, we found that with different electrode arrays and at different sites the potential errors demonstrate a general property, which may be regarded as a negative-power function of potential reading. Power net transients, background telluric variation and instrument malfunction are possible sources that may cause the large errors present as outliers deviating from this function. We reaffirm the fact that the outliers are often correlated with high contact resistances for some of the electrodes used in a measurement, but this may also be caused by an unsatisfactory connection between the electrode and the cable due to, for example, dirt or oxide on the connectors. These outliers are often the main part of the errors affecting the imaging results. Furthermore, a robust inversion and a smoothness-constrained inversion were applied to the investigation of the effects of the measurement errors. Using two real data sets, we show that the smoothness-constrained least-squares inversion is much more sensitive to the potential errors than the robust inversion, but the two inversion schemes produce very similar models with a high data quality. Artefacts or indefinite parts in the inverted models correlate with the distribution zones of the outliers in the potential error pseudosection.

INTRODUCTION

In the last decade, there has been great progress in computerized data acquisition systems and 2D and 3D inversion software for DC resistivity measurements. Resistivity tomography or imaging is now widely employed in environmental investigation and civil engineering (i.e. Van *et al.* 1991; Dahlin 1996; Olayinka and Yaramanci 1999; Chambers *et al.* 1999). As is well known, the quality of the observed data or noise contamination mainly affects the resolution and reliability of the technique and it depends on all aspects of the fieldwork. To apply the imaging technique success-

* bing.zhou@adelaide.edu.au

fully, great attention must be paid to controlling the observed data quality in fieldwork and data processing, and any possibilities of minimizing the effects from all kinds of error sources must be taken. For this reason it is important to investigate the properties of the data observation errors and understand their effects on the imaging results.

In general, the measurement errors studied here may be simply classified into two kinds of measurement error-electrode spacing errors and observed potential errors, which are the main factors in calculating the apparent resistivity or resistance for 2D resistivity imaging. The electrode spacing error is caused by the measurement error in electrode positions or inadvertent electrode setting-up, which hopefully is minimized by careful work by the data acquisition field crew. In most cases of 2D resistivity imaging surveying, multi-electrode cables with fixed spacing, e.g. 5 m or 10 m, are employed along a measurement line. However, it is not uncommon that some portions of the cables cannot be straightened due to rough terrain or vegetation, or the positions are shifted to improve electrode contact with the ground. Sometimes the electrode positions are measured with a string or tape, with the associated risk of electrode spacing errors due to the human factor. Thus, it is easy to envisage, for example, a 10% spacing error when using an electrode separation of 1 or 2 metres, at least if the field crew is not fully aware of the importance of keeping the electrode separations as exact as possible. On the other hand, for resistivity imaging surveying in a practical situation one specific electrode array is normally chosen, such as the pole-pole, pole-dipole, dipole-dipole, Wenner or Schlumberger array. These arrays employ specified electrode configurations in a measurement line. Due to the difference between the electrode configurations, the spacing errors of these arrays may affect the observed potentials or apparent resistivities in different ways. To obtain a high quality subsurface image, it is necessary to evaluate the spacing error and its effect on imaging quantitatively so as to minimize the spacing-error-related artefacts in the inverted model.

The potential error arises from many sources, such as bad electrode contact, cable insulation damage, site background noise (telluric current and power line noise), instrumental problems (the wrong current injection and picking-up of noise potentials) and improper instrument operation. Some of these error sources are unpredictable and occasional incidents. To evaluate the potential errors of a pole-pole array, Park and Van (1991) conducted field experiments with the reciprocity principle and found that about 15% of their data did not satisfy reciprocity, and that the finite noise contribution introduces a systematic error into inversion. LaBrecque *et al*. (1996) investigated the effects of noise on Occam's inversion for resistivity tomography and emphasized that under-estimated noise may cause the inversion to fail in achieving an adequate data fit, the resulting imaging becomes rough and artefact-contaminated. On the other hand, over-estimated noise may substantially decrease the imaging resolution (the image is too smooth). Knowledge of the data quality or the noise level of data is crucial to the successful application of resistivity imaging. So, close attention must be paid to estimating the error levels of data and the effects on imaging results. In principle, two methods may be adopted to check the data quality. One is to repeat the observation at the same point in order to calculate the mean, or median value and the standard deviation as an error estimate for the data point in question. However, it has been observed in practical applications that data outliers may result from highly stable repeated data, which may be caused by, for example, capacitive coupling effects, so a low standard deviation does not guarantee good data quality. Another alternative is the use of normal and reciprocal measurements at the same point (Park and Van 1991; Van *et al*. 1991). Theoretically, without any noise the normal and reciprocal measurements should give same observed values, so the difference between the two measurements will give an estimate of the measurement errors. This data quality control can be efficiently fulfilled by an automatic data acquisition system for all the data-points in a measurement, although at the cost of increased measuring time.

In recent years, we used our automatic DC data acquisition system, a modified version of the Lund Imaging System (Dahlin 1993) using a 24-bit sigma-delta A/D-converter as receiver, and collected resistivity data successively in normal and reciprocal modes at several sites in Sweden and overseas. These data allowed analysis of the properties (distribution patterns and magnitude) of the observed potential errors in normal and reciprocal surveys, and their effects on the imaging results with different inversion schemes. In this paper, we first carried out analytical experiments to evaluate quantitatively the magnitude and appearances of the in-line and off-line spacing error for different electrode configurations in 2D resistivity imaging surveys. Then, we showed the distribution patterns and statistic properties of the observed potential errors obtained by the normal and reciprocal readings at different sites in Sweden and overseas. Finally, we carried out robust and smoothness-constrained least-squares inversions with synthetic data and two field data sets so as to show the effects on the images due to the spacing errors and the potential errors.

ELECTRODE SPACING ERROR

Theoretically, the electrode spacing error may be analytically evaluated by the geometry factor of a specified array, i.e. for surface surveys the geometry factor can be written in the following general form:

$$K = \frac{2\pi}{f_A - f_B}, \quad (1)$$

where $f_\varsigma = 1/r_{\varsigma M} - 1/r_{\varsigma N}$, the subscripts A, B, M and N represent the four electrodes of an array and $r_{\varsigma M}$ denotes the distance between points ζ and M. If any of the electrodes is remote we take $r_{\varsigma B} = \infty$ or $r_{\varsigma N} = \infty$. From equation (1) we obtain the estimate:

$$dK = \frac{K^2}{2\pi}\left[\left(\frac{dr_{BN}}{r_{BN}^2} - \frac{dr_{BM}}{r_{BM}^2}\right) - \left(\frac{dr_{AN}}{r_{AN}^2} - \frac{dr_{AM}}{r_{AM}^2}\right)\right] \quad (2)$$

due to the spacing error dr_{AM}, dr_{AN}, dr_{BM} or dr_{BN}. For example, the simplest case is the pole-pole array ($r_{BN} = \infty$ and $r_{BN} = \infty$), which only involves two points A and M. Assuming they are located at $(x_A \pm \Delta x, 0, 0)$ and $(x_M, 0, 0)$, where Δx is the spacing error in the x-direction (called an in-line spacing error), we have the substitutions $dr_{AM} = \pm\Delta x$ and $r_{AM} = |x_A - x_M|$ for equation (2) and obtain the error in the geometry factor: $dK = \pm 2\pi\Delta x$. In the same way, $dK = \pi\Delta y^2 / |x_A - x_M|$ and $dK = \pi\Delta z^2 / |x_A - x_M|$ can be obtained due to the spacing errors in the y- and z-directions, respectively (both are termed the off-line spacing errors). From this example, it can be seen that the off-line spacing error is much smaller than the in-line spacing error because of $|x_A - x_M| >> \Delta z, \Delta y$. Table 1 gives all the analytic estimations of the in-line spacing error for common electrode arrays and it shows that the pole-pole, pole-bipole, Wenner and Wenner-β surveys are rather insensitive to the spacing errors (independent of n) but the dipole-dipole array is much more sensitive than the others, because the geometry factor change due to the spacing error is proportional to n^3, where n is the factor of separation between the current and potential electrodes. The above analytic estimation is based on a homogeneous half-space, or calculation of apparent resistivity. In a practical application of 2D resistivity imaging the subsurface is not homogeneous, and hence equation (2) cannot give the whole picture of the spacing error in a resistivity imaging survey. Here, we applied another method to simulate the spacing errors in inhomogeneous subsurfaces to evaluate the spacing error in a 2D resistivity imaging survey. For easy and exact calculation of the difference between the potentials due to the small spacing errors, we chose a two-layered model and a vertical contact whose solutions may be analytically obtained. We assigned resistivities of $\rho_1 = 10\ \Omega$m and $\rho_2 = 100\ \Omega$m to the two models, and calculated the resistances with correct electrode positions and some incorrect electrode positions, then plotted the results as a pseudosection so as to view the whole appearance of the spacing error. We found that the error effects with the two inhomogeneous models are very similar. As an example, Fig. 1 gives the simulation results of the in-line spacing errors for the two-layered model (note the different scale used for the different electrode array types). In these simulations, we assumed that four electrodes locating at (22, 0), (33, 0), (53, 0) and (61, 0) have 10% negative or positive x-position errors relative to the basic spacing of 1 m. Obviously, Fig. 1 shows that the spacing errors of the different electrode configurations may affect the observed data (apparent resistivity or resistance). Due to different radiating patterns from the erroneous electrodes, the negative and positive errors have different sized effects on the observed data, and the magnitude of the effects decreases along the radiating paths (actually with the spacing of electrodes in surveying). Also, it shows that γ-array, dipole-dipole and Wenner-β configurations have over ±20% relative error due to the 10% in-line spacing error, and other configurations have around the same levels as the spacing errors. This means that these three arrays may have effects on the in-line spacing errors that are twice as large as those of the other configurations. We also simulated the off-line spacing

Array	**Geometry factor change due to the spacing error**: $\bar{\varepsilon} = \pm\{\Delta x_A, \Delta x_B, \Delta x_M, \Delta x_N\}^T$
Pole-pole	$2\pi\{-1, \quad 1, \quad 0 \quad 0\}\varepsilon$
Pole-dipole (n=1,2,…) Pole-bipole (n=1)	$2\pi\{-(2n+1), \quad (n+1)^2, \quad -n^2, \quad 0\}\varepsilon$
Wenner (n=1) Schlumberger (n=1,2,…)	$\pi/2\{-(2n+1), \quad 2(n^2+n)+1, \quad (2n+1), \quad -2(n^2+n)-1\}\varepsilon$
Dipole-dipole (n=1,2,…) Wenner-β (n=1)	$\pi/2\{-(2n+1)(n+2)^2, \quad (2n+1)(n+2)^2, \quad n^2(2n+3), \quad -n^2(2n+3)\}\varepsilon$
γ-array (n=1,2,…)	$\pi\left\{-\frac{n^2(n+1)(n+3)}{2(n^2+n-1)^2}, \quad \frac{(n^2+1)(n+2)^2}{2(n^2+n-1)^2}, \quad \frac{-(n^2+1)(n+2)^2}{2(n^2+n-1)^2}, \quad \frac{n^2(n+1)(n+3)}{2(n^2+n-1)^2}\right\}\varepsilon$

Table 1

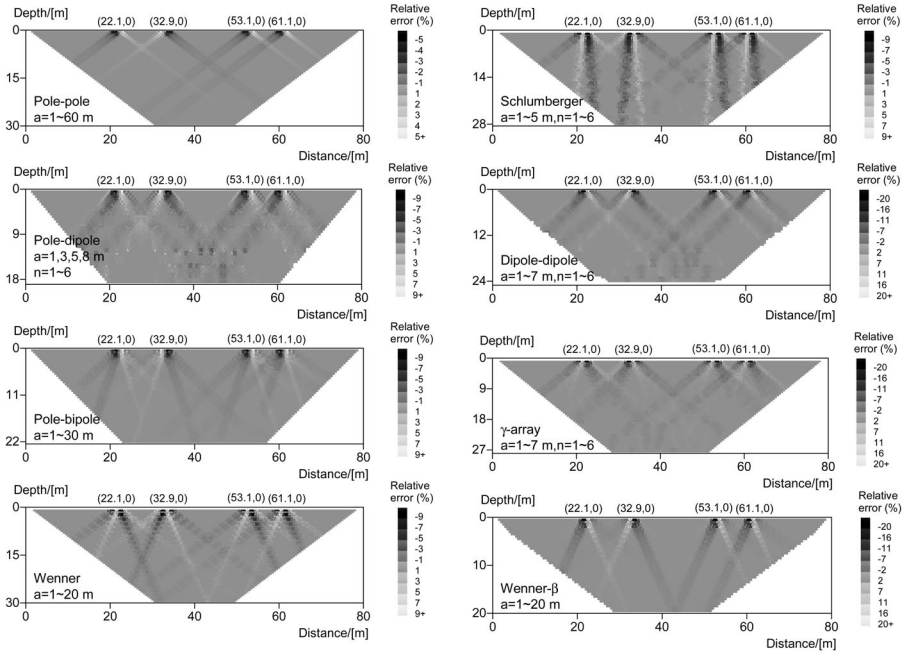

FIGURE 1
Pseudosections of the in-line spacing errors due to the incorrect positions of four electrodes. 10% spacing errors were assumed here, which may cause a more than 20% resultant effect on the dipole-dipole, Wenner-β and γ-array data.

error with the four erroneous electrodes (omitted here) and found that the effect creates patterns of the off-line spacing error very similar to Fig. 1, except that the negative and positive spacing errors have the same effect values (negative), and the maximum effect values for γ-array, dipole-dipole and Wenner-β surveys did not reach 2%. They are much smaller than the in-line spacing errors where they reach over 20%. For any other inhomogeneous structure, the spacing error should have the same properties as shown in Fig. 1, which gives the specified spreading patterns of the spacing error for different electrode array surveys. From this it is understandable that small fixed perturbing sources, such as, for example, blocks of rocks or small clay lenses, may have the same effect patterns as the spacing errors, but the magnitudes may be different and depend on the difference in electrical properties.

OBSERVED POTENTIAL ERROR

As mentioned above, the observed potential error may arise from different sources and it may deviate at different sites, different times and with different data acquisition systems. An efficient way to evaluate the data quality is to repeat the measurements using the reciprocity principle at the field sites. For some electrode arrays the noise in the reciprocal measurements can be expected to be larger than for the normal measurements, due to the much longer potential electrode separation that will be more prone to pick up noise. This applies to, for example, the Wenner, Schlumberger and pole-dipole arrays. For the dipole-dipole array, on the other hand, the normal and reverse arrays are simply mirrored and therefore should not differ in noise characteristics in general. Thus, the normal and reciprocal measurements will

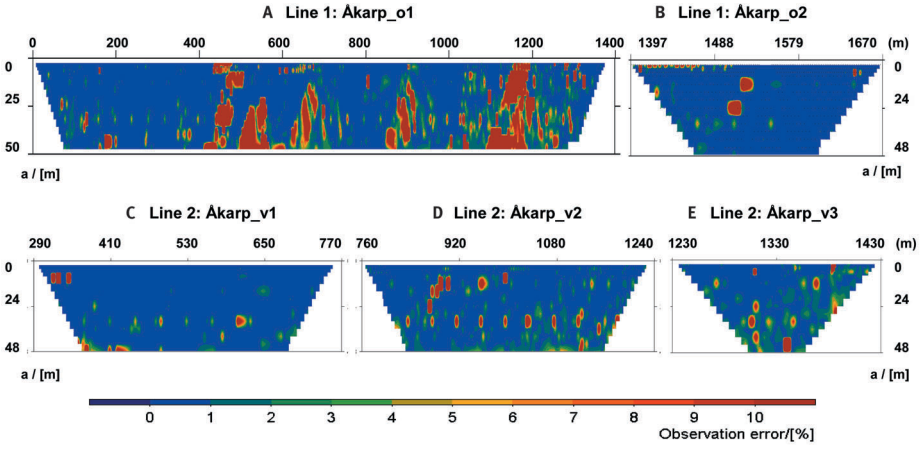

FIGURE 2
Error pseudosections from normal and reciprocal Wenner measurements at the Åkarp site, southern Sweden. This shows that the larger relative errors may appear with large and small potential electrode separations, and possibly indicate where the perturbing sources were in the 2D resistivity imaging survey.

give a conservative estimate of the data quality. Fortunately, several commercial automatic data acquisition systems are now available to carry out the job efficiently so that we can check the data quality, investigate the properties of the errors and evaluate the effect on the imaging results. The following paragraphs give some examples of error analysis of field data collected in recent years, which have been selected since they represent examples of data with quality problems due to, for example, high contact resistances or ambient noise. All the data sets were obtained using a modified version of the ABEM Lund Imaging System (Dahlin 1993), where the potentials are measured with a Lawson Labs model 201 24-bit sigma-delta A/D-converter. This instrument set-up has generally proved to provide data of very high quality, so the noise estimates may not be relevant to data measured with instruments of poorer resolution and noise suppression. Under surveying conditions normally encountered outside urban areas in southern Sweden, the average errors estimated from reciprocal measurements fall well below 1% with this equipment.

For the examples presented below, each data point was automatically repeated with the normal and reciprocal electrode configurations. The absolute relative error of the measurements was calculated in order to obtain the statistic properties and a potential error pseudosection (plotting the relative error in the same way as used for apparent resistivity pseudosection) to view the data quality.

Åkarp site

This site is located at the railway station of Åkarp village in southern Sweden, where two parallel lines (namely Line 1 and Line 2) of Wenner resistivity imaging measurement along 1670 m of railway track were carried out as a geotechnical investigation. Line 1 has two segments (Åkarp_o1, Åkarp_o2, see Fig. 2a,b) on one side of the track and Line 2 is shorter than Line 1 but consists of three parts (Åkarp_v1, Åkarp_v2 and Åkarp_v3, see Fig. 2c,d,e) on the other side of the same track. In order to complete the surveys within the available time limits, only one measurement was taken for each data point to allow the reciprocal data to be included, so if normal data would have been measured and repeated the data quality may have been slightly better. Figure 2 gives the pseudosection of the absolute relative error of the two lines and it shows where the large potential errors (outliers) are located. Figure 3 shows the logarithmic plots of the potential errors against the measured potentials. Each plot in Fig. 3 gives the line length, data points and statistical properties, such as mean values (ε), standard deviation (σ) and least-squares regression function (β). From Figs 2 and 3, it can be seen that the first part of Line 1 (Åkarp_o1) has many more outliers (see Fig. 3a: it has 551 data points larger than 10% and the standard deviation reaches σ=20.1%) than others and most of them are distributed in four dipping zones of about between the sections x=400–600 m, x=610–700 m, x=850–925 m and x=1100–1200 m (see Fig. 2a). This feature is similar to the distribution of the spacing errors (see Fig. 1) and it implies that some of the fixed perturbing sources were close to the line. Also, it shows that the larger relative errors (outliers) may appear with large as well as small spacings in the measurements, and mainly depend on the potential readings between the electrodes. In fact, we found that the sources of disturbance

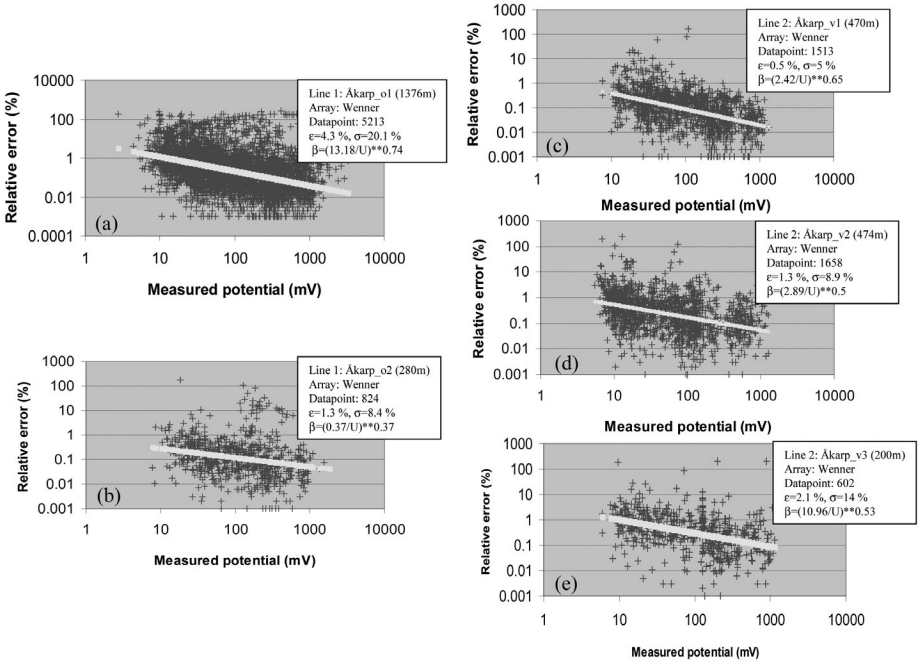

FIGURE 3
Logarithmic plots of the potential errors from normal and reciprocal measurements at the Åkarp site, southern Sweden. Line 1: (a) Åkarp_o1 and (b) Åkarp_o2; Line 2: (c) Åkarp_v1, (d) Åkarp_v2 and (e) Åkarp_v3. This shows that the data qualities may vary in different parts of the measurement, and the outliers may occur in the whole range of the potential readings, but the potential error generally increases as a power with the decrease of the potential readings.

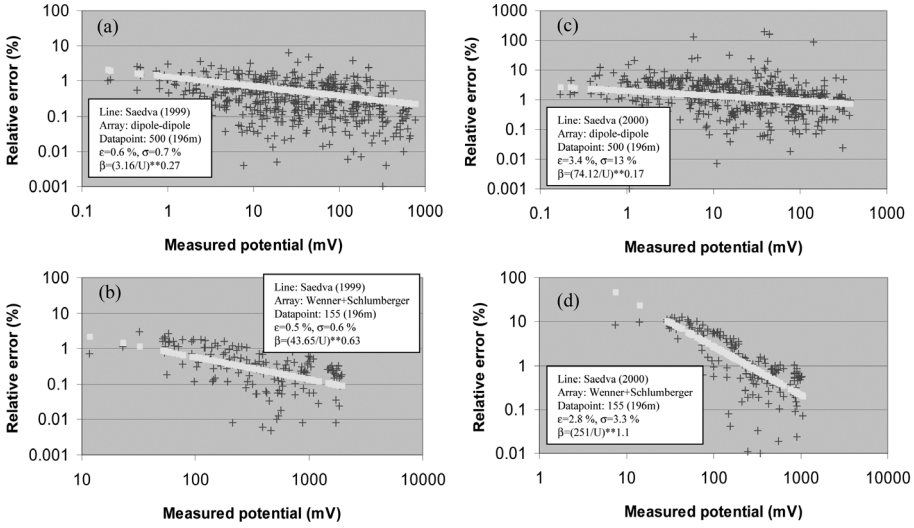

FIGURE 4
Logarithmic plots of the potential errors from normal and reciprocal measurements at the Sädva dam, northern Sweden. (a) Dipole-dipole survey in 1999, (b) Wenner+ Schlumberger survey in 1999, (c) dipole-dipole survey in 2000, (d) Wenner+Schlumberger survey in 2000. These show that high data quality may be obtained with both dipole-dipole and Wenner measurements for monitoring dam safety, although the dipole-dipole data may have larger potential errors than does the Wenner data for measurements with the same background.

could be high-resistance paving (e.g. at x=1100–1200 m) under a surface cover of grass. However, electrical disturbance from the power supply system of the railway is also a possible source of noise, and metal fences or grounded metal objects near the current and potential electrodes probably also contribute to the man-made noise. Line 2 and Åkarp_o2 present much better data qualities than Åkarp_o1. Their mean values (ε = 0.5~2.1%) and standard deviations (a = 5~14%) were almost half compared to Åkarp_o1 (ε = 4.3%, σ = 20.1%). They have less than 3% of data points with errors larger than 10% and over 90% of data points have errors less than 2%, and the outliers are sparsely and irregularly distributed in the pseudosections (see Fig. 2b,c,d,e). All of these features indicate that the instrument works quite well during the measurements and the background noise (i.e. telluric and other leaking current sources) seems to have a limited influence on the observations. From Fig. 3, it can also be seen that the statistical distribution of the relative errors can be described by a negative power function (β) of the potential reading (see yellow line in the diagrams of Fig. 3), which basically gives the quantitative relationship between the observation error and the measured potential. This regression function shows that the error increases as a power with the decrease of the potential reading, which means that the signal strength of the measurement is very important in controlling the data quality. It also shows that the outliers may occur over the whole range of the measured potentials (see Fig. 3) and the different parts of a measurement campaign in the same area may have varying data quality, i.e. the five parts of the two lines give different regression functions, but the slopes (power number) of the regression lines did not change much (0.4~0.7), which indicates that the background noise affects the five parts mostly in the same manner. Most of the outliers in Fig. 3a came from the fixed perturbing sources.

Sädva Dam

In order to detect internal erosion and seepage variation in an embankment dam, an electrical monitoring system was installed at the Sädva dam in northern Sweden (Johansson *et al*. 2000). This installation includes 96 steel plate electrodes (32 on the main dam and 64 on the side dam) with 6 m spacing, and 32 non-polarizable SP-electrodes with the same spacing but shifted 3 m relative to the steel electrodes in the main dam. Figure 4 shows examples of data quality analysis of the resistivity measurement with dipole-dipole and Wenner+Schlumberger arrays in the first year (1999) and second year (2000) after installation. From this figure it can be seen that the data quality in 1999 is excellent with both dipole-dipole and Wenner+ Schlumberger arrays (see Fig. 4a,b), and the mean values and standard deviations of relative error were both less than 1%, but in 2000 the data quality changed with the mean value variation increasing from less than 1% to around 3% and the standard deviation increasing from 0.6% to 13%, especially with the dipole-dipole array (see Fig. 4c,d). Also, it can be seen that a few outliers of the errors appear with the dipole-dipole array in the second year and the slope of the regression line of the Wenner+Schlumberger array became much larger than before. By plotting the error pseudosections (not shown here) we found that the locations of the outliers were distributed irregularly in the pseudosection, indicating that they possibly came from the arbitrary background noise. From the statistical properties point of view, the relative error change did not seriously affect the data quality (ε=2.8~3.4%), indicating that the background noise was low. It may be noted, though, that the current transmitter broke down immediately after the second data set was recorded, and it is not unlikely that its behaviour was somewhat erratic during the survey. Furthermore, it is possible that the uppermost part of the dam core, where the electrodes are

placed, was still partially frozen after the winter during the second year survey. This is supported by the fact that the contact resistances were higher than in the previous survey. Nevertheless, these examples once again show that the relative error generally increases in a negative exponent with the measured potential of these three electrode configurations. Meanwhile, the dipole-dipole array had a larger mean value and standard deviation than the Wenner and Schlumberger measurements, due to the relative small strength of the measured potential. However, the dam monitoring measurement shows that high data quality can be obtained with these three electrode configurations.

Nyamandhlovu area, Zimbabwe

Three lines of resistivity imaging for investigation of groundwater were carried out in the Nyamandhlovu area, 50 km to the northwest of the city of Bulawayo, Zimbabwe (Andersson and Engman 2000), where a hydrogeological study indicates the presence of deep confined aquifers in sedimentary sequences with tectonic structures. As an example, Fig. 5 shows the observed potential errors of the Wenner and Schlumberger measurements along Victoria Falls Road in the area. Also, at this site, stacking data using a normal array were substituted by taking reciprocal measurements additionally, but without stacking the data. From Fig. 5a, it can be seen that the mean value and the standard deviation of the potential error reach 11.8% and 32.3%, respectively, and many errors larger than 10% occur in the small potential range (< 10 mV, see Fig. 5a) and mostly in the two distance intervals x=1100–1400 m and x=1800–2200 m (see Fig. 5b). The two outlying zones started from a=40 m spacing to the maximum spacing in the two sections. Obviously, Fig. 5b shows that the data quality of the first half of the line (x=0–1000 m) was much better than the second half of the line (x=1000–2200 m). In fact, the appearance of the errors is related to the surface geology (Andersson and Engman 2000). Weathered basalt with favourable electrode contact dominates from x=0 m to x=800 m, after which the soil becomes more sandy and the Kalahari sand appears from x=1100 m and continues until the end of the line at x=2200 m. The Kalahari sand has much higher resistivity than the weathered basalt, so it gave high contact resistances in this part.

EFFECTS ON IMAGING RESULTS

As is well known, the final step of the data processing in resistivity imaging is to conduct an inversion with some criteria of data fit and model roughness, such as the robust inversion (Claerbout and Muir 1973; Wolke and Schwetlick 1988; Madsen and Nielsen 1993), the smoothness-constrained least-squares inversion (DeGroot-Hedlin and Constable 1990; Sasaki 1992), the smoothest model inversion (Constable *et al.* 1987; Ellis and Oldenburg 1994; Oldenburg and Li 1994) and the subspace inversion (Skilling and Bryan 1984; Kennett and Williamson 1988; Oldenburg *et al.* 1993). Methodologically, all these inversion schemes may incorporate information about the data quality, for example, if the observation error or standard deviation σ_i of each datum is known, a weighting operator or a weighting matrix $W_d = diag\,[1/\sigma_1, 1/\sigma_2 \ldots, 1/\sigma_N]$ can be applied to the inversion schemes and the reconstructed model can be obtained with this information taken into account. For example, LaBrecque *et al.* (1996) showed one such inversion but they emphasized the necessity of knowing exactly the

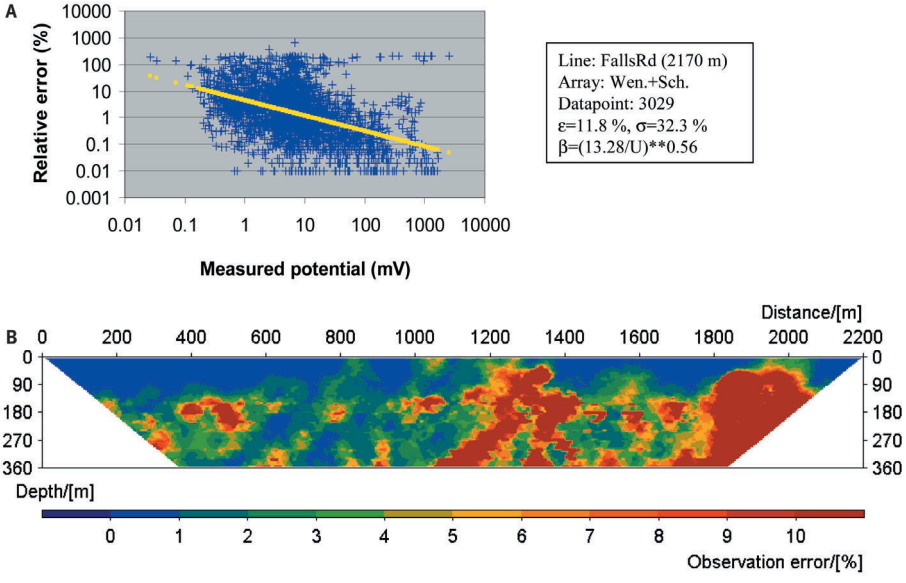

FIGURE 5
Logarithmic plot (a) and pseudosection (b) of the potential errors from normal and reciprocal measurements at a Zimbabwe site.

error levels of the data for a reasonable image, otherwise under-estimated or over-estimated noise may fail in achieving good data fit or decrease the imaging resolution. In theory, the standard deviation σ_i should be obtained from field measurements for each data point in a statistic sense. Unfortunately, in practical applications it is often not feasible to obtain all these values $\{\sigma_i, i=1,2,\ldots, N\}$ for the data quality information, due to time and economical constraints in the data acquisition. However, the logarithmic plots and the potential error pseudosections shown in the previous section do provide an overview of the data qualities with which we can investigate the effect of the errors on the inverted model. Two inversion schemes, the robust inversion (Wolke and Schwetlick 1988) and the smoothness-constrained least-squares inversion (DeGroot-Hedlin and Constable 1990; Sasaki 1992) were used in this work. Both schemes are built into the commercial resistivity imaging software, *RES2DINV*, as two options. In principle, the smoothness-constrained least-squares inversion seeks the smooth model that has a minimum data misfit with the squared residuals (L_2-norm). It tends to be more influenced by data points with a larger misfit, which makes it sensitive to the data outliers. A robust inversion means finding the model that gives the best misfit of the absolute values of the data residuals. This approach leads to the data outliers having less influence. We used the difference of the two inversion schemes as a tool for investigating the effect of the measurement errors. All the inverted models shown in the following sections are the results after six iterations of the two inverse schemes with the same appropriate inversion parameters (optimal damping factors).

Synthetic data

Firstly, to investigate the effect of the spacing error we applied the two inversion schemes to the synthetic data of the three models we used previously: a homogeneous model, a two-layered half-space and a vertical contact. The 'observed data' were contaminated by in-line spacing errors of 10% at the four electrodes shown in Fig. 2. The inversion results show that the three electrode arrays, dipole-dipole, γ-array and Wenner-β, have four apparent artefacts just below the four erroneous electrodes in the inverted models produced by the both inversion schemes, where Fig. 6 gives the inverted models for a homogeneous model and a two-layered half-space. Other electrode arrays did not yield such large artefacts. This is because the effect on the resistivity data due to the 10% in-line spacing error is much larger for these three electrode arrays than for the other arrays (see Fig. 1). Our other experiments (not shown here) indicate that with the increase in the spacing error, i.e. larger than 10%, the artefacts are more visible, but their positions do not change. This feature implies that the effect of the spacing error is similar to small 3D fixed disturbances close to the electrodes, such as, for example, small-scale near-surface geological variations. Understandably, the disturbances may yield analogous artefacts in the inverted models. These experiments imply that when working with these three arrays for resistivity imaging, one should minimize the in-line spacing error, and if possible the disturbances from other small-scale near-surface geological variation in the field, so as to remove the artefacts in the inverted models. The other arrays seem to have much less sensitivity to the spacing error and the small-scale disturbances than do the

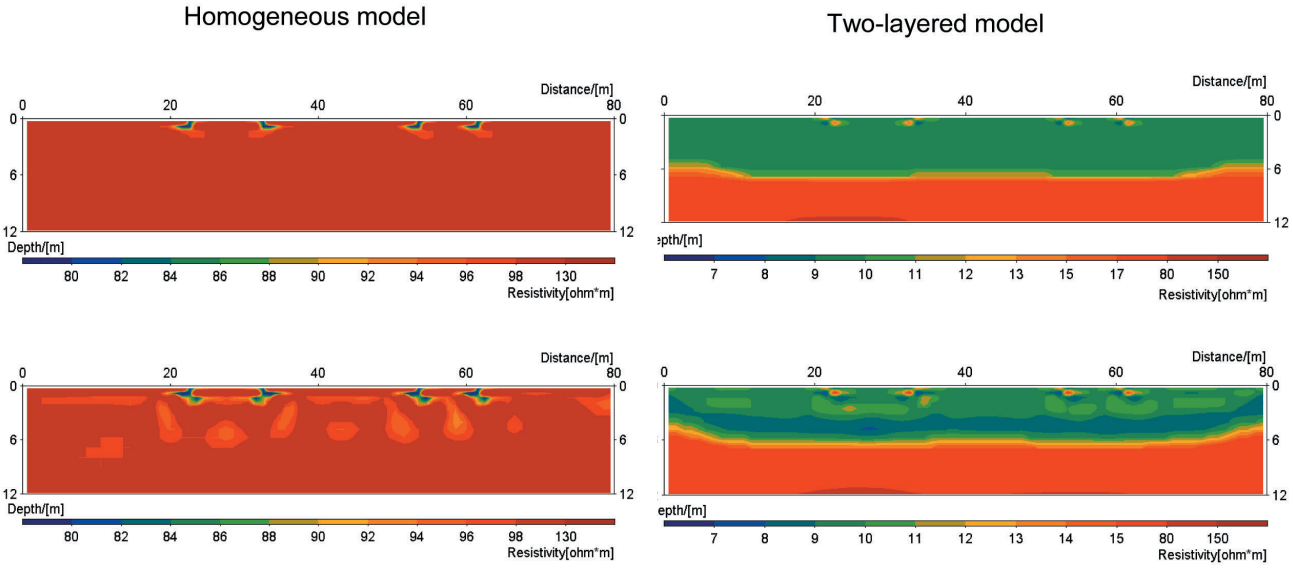

FIGURE 6

Artifacts of the in-line spacing errors shown in Fig. 1, with dipole-dipole data for a homogeneous model (left panel) and a two-layered model (right panel). The upper two diagrams were obtained by robust inversions and the lower two diagrams were produced by the smoothness-constrained least-squares inversions.

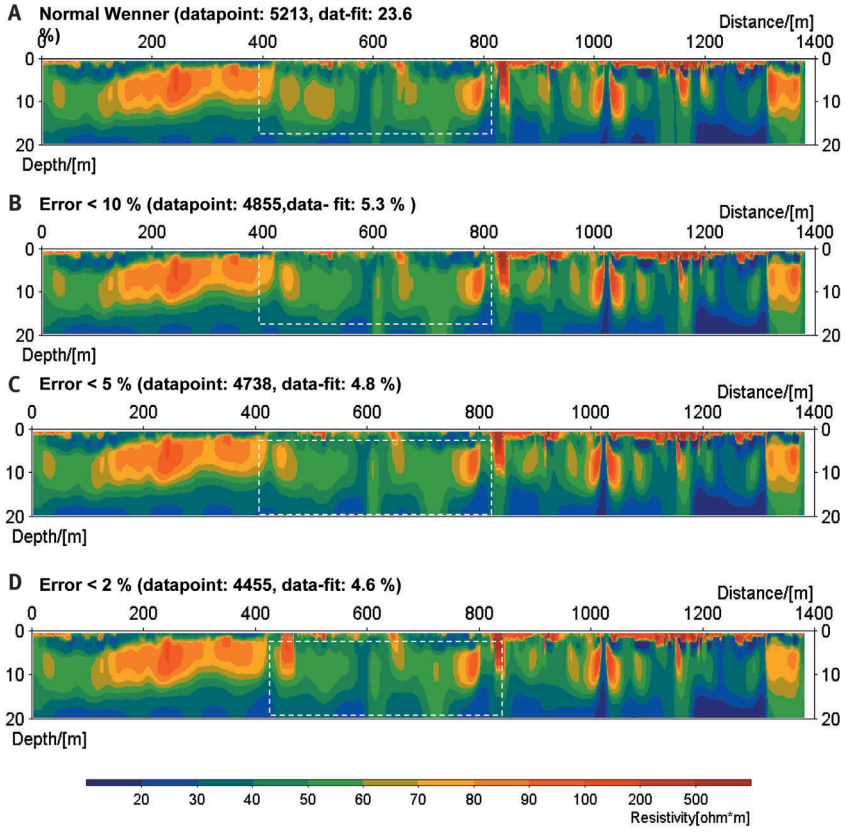

FIGURE 7
Inverted models of the robust inversion (L_1-norm) for Åkarp_o1 with different potential error levels from normal and reciprocal measurements. The inverted models were obtained using the normal measurement data that contain all the noise (a) and the partial data whose potential errors were less than 10% (b), 5% (c) and 2% (d).

three arrays. The appearance of the artefacts in the inverted model may help us to recognize the false images due to the spacing error or small-scale near-surface variations for interpretation of field data.

Field data

In order to investigate the effect of the potential error discussed in the previous section, we also applied the two inversion schemes to all the field data sets with different levels of the errors. The investigation was carried out with the following procedure: Firstly, we applied the two inversion schemes to the normal surveying data that probably contain all the noise, we then repeated the inversions after individually removing the data points whose relative errors are larger than 10%, 5% and 2% according to the logarithmic plots and potential error pseudosections. Actually, in this procedure we assumed that the data having larger relative errors (outliers) shown in the logarithmic plot or the potential error pseudosection were 'bad data' for the inversions even though the reciprocal measurement was more prone to pick up noise due to the longer potential electrode separation. However, this procedure enabled us to obtain a sequence of inverted models with different error levels and to view clearly the effect of the potential errors on the inverted models. Two data sets were specifically shown in the following. One data set was chosen from the first part of Line 1 at the Åkarp site, southern Sweden, known as Åkarp_o1, whose relative potential errors are given in Figs 2a and 3a. Another data set was chosen from the line at the Zimbabwe site shown in Fig. 5. These two data sets have relative large mean values and standard deviations of the potential errors compared with the other data sets presented above (see Figs 2–5), which show good data quality and for which the inverted models from both inverse schemes gave consistent features in the resistivity structures.

Åkarp site

Figure 7 shows the robust inverted models for Åkarp_o1 with the different potential error levels. For each inverted model the number of data points, the potential error level and the absolute error of the data misfit are specified. From these results, it can be seen that the four inverted models obtained with different levels of potential errors have nearly the same basic features in the reconstructed images. They show that with the decrease in the error levels from the original (about 7% data points are larger than 10%) to all the data points less than 2%, the four inverted models were not significantly changed. The whole line can be divided into three parts. The first part, x=0–400 m, consistently presents a three-layered structure in which there is a resistant layer between the depths z=3 m and z=15 m. From Fig. 2a, the error distribution indicates that this part has good data qual-

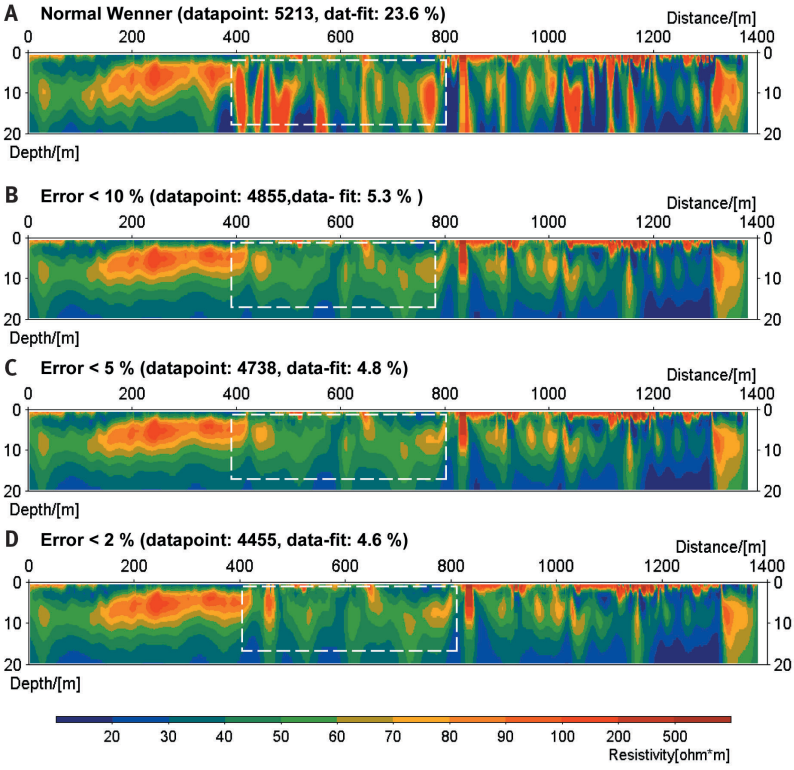

FIGURE 8
Inverted models of the smoothness-constrained least-squares inversion (L_2-norm) for Åkarp_o1 with different potential error levels from normal and reciprocal measurements. The inverted models were obtained using the normal measurement data that contain all the noise (a) and the partial data whose potential errors were less than 10% (b), 5% (c) and 2% (d).

ity (a few outliers, over 90% data points < 1%). The second part, x=400–800 m, presents a slight change (see dash-lined zone in Fig. 7). With the decrease in the error levels, two narrow resistant blocks gradually appear at x=450 m, x=650 m, near the surface. This slight change could be related to the outliers of the potential errors in this part (see Fig. 2a) and the narrow resistant blocks may be the distorted images of fixed perturbing sources near the line (i.e. the pavement mentioned above), due to the high-contrast electric properties and the 2D approximation in the inversion. These fixed disturbances are probably the sources of the outliers in the error pseudosection (see Fig. 2a). The third part from x=800 m to the end of the line (x=1400 m) obviously gives an ambiguous image of this part in all four inverted models. There appears to be a thin top layer of high resistivity and below that the resistivity structure is indefinite due to being cut off by several resistant or conductive 'dykes' at x=820 m, x=1020 m and x=1150 m. These 'dykes' are probably the distorted images of the nearby disturbances (fence and pavement lenses). The similarity of the four models in this section indicates that a number of outliers in this part (256 data points > 5%, see Fig. 2a) did not significantly affect the inverted models, based on the normal Wenner measurements, and they are dominated by noise picked up in the reciprocal measurements only. But the deviation of the measurements at least shows that there must be either significant differences in the electrode contact resistances between the normal and reciprocal measurements, or disturbances that cause so many outliers for the reciprocal survey in this part. Due to these disturbances or bad electrode contacts, the inverted model of this part actually gives an ambiguous image even though the normal data did not contain the majority of the outliers shown in Fig. 2a. However, this implies that the distribution of the outliers from the reciprocal measurement will give information on 'good' or 'bad' surveying situations.

Figure 8 shows the inverted models of the smoothness-constrained least-squares inversion with different potential error levels. Comparing Fig. 8a with Fig. 8b,c,d, it can be seen that the section starting from x=0 m to x=400 m presents a clear and stable three-layered structure in all four models, which is consistent with the results from the robust inversion (see Fig. 7). The clearness and the consistency obviously relate to the good data quality in this section (see Fig. 2a, over 90% data points < 2%). But the image of the second section, x=400–800 m in Fig. 8a, obviously differs from the other images (compare dash-lined zone in Fig. 8a and Fig. 8b,c,d). Some artefacts or distortions can be seen in this part of Fig. 8a but they disappear with the low error levels. Referring to Fig. 2a, it can be seen that these artefacts or distortions correlate with the distribution of the outliers in the error pseudosection. The appearance of the artefacts shows that the outliers affect the inverted model and the data from the normal survey were really contaminated by these error outliers. The last section, x=800–1400 m, of the four models shows no significant change with the error levels and it is

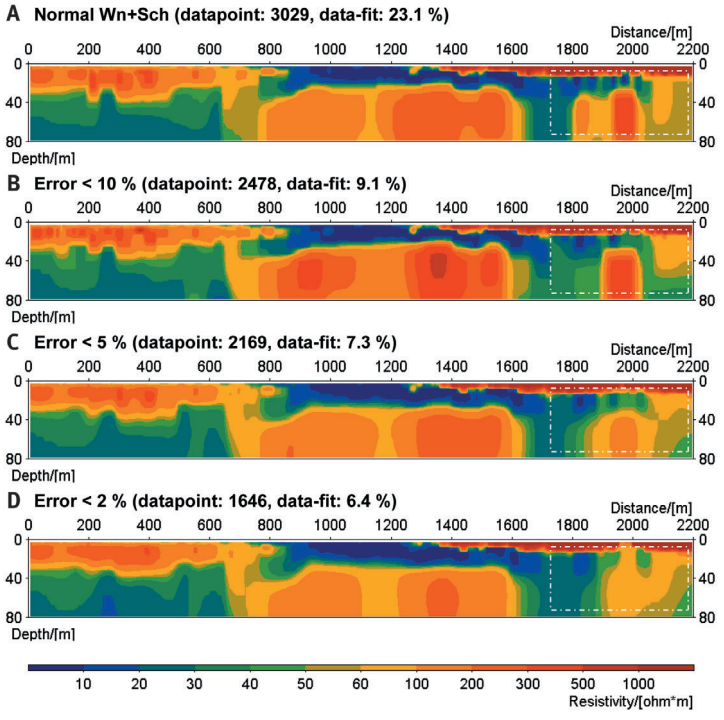

FIGURE 9

Inverted models of the robust inversion (L_1-norm) for the Zimbabwe site with different potential error levels from normal and reciprocal measurements. The inverted models were obtained using the normal measurement data that contain all the noise (a) and the partial data whose potential errors were less than 10% (b), 5% (c) and 2% (d).

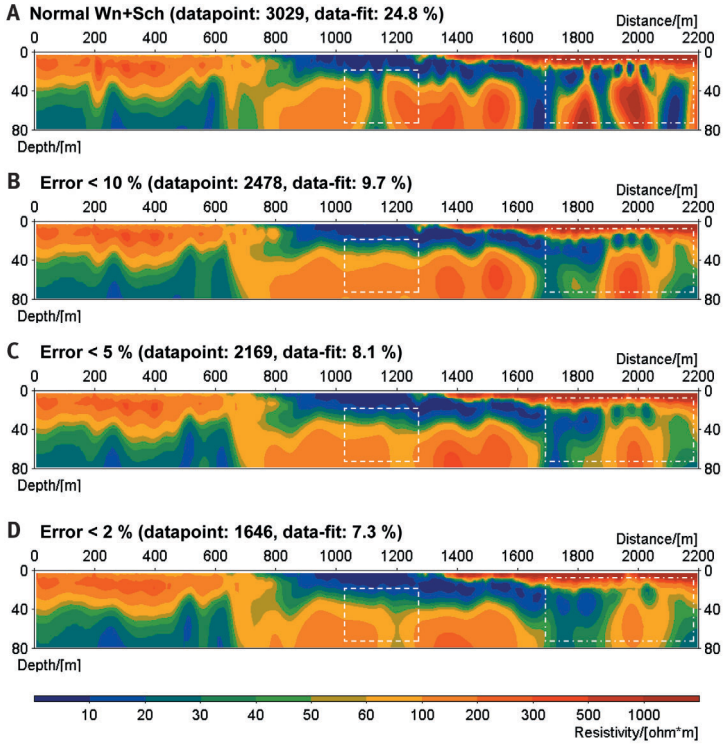

FIGURE 10

Inverted models of the smoothness-constrained-least squares inversion (L_2-norm) for the Zimbabwe site with different potential error levels from normal and reciprocal measurements. The inverted models were obtained using the normal measurement data that contain all the noise (a) and the partial data whose potential errors were less than 10% (b), 5% (c) and 2% (d).

very similar to the results of the robust inversion (see Fig. 7). This means that the outliers in this part (see Fig. 2a) did not seriously affect the inverted models, the data from the normal survey in this part did not contain the majority of these outliers and thus most of them came from the reciprocal measurements. In addition, comparing Fig. 7b,c,d with Fig. 8b,c,d, it can be seen that the inverted models from the two inversions become very similar and the data misfits from the robust inversion were slightly better than those from the smoothness-constrained least-squares inversion (the data misfit was evaluated by the squared average of relative errors). This example indicates that the smoothness-constrained least-squares inversion is much more sensitive to the outliers that appeared in the error pseudosection (Fig. 2a) than the robust inversion, and the two inversion schemes may give similar images with high data qualities. This means that when applying the smoothness-constrained least-squares inversion, one should remove all the outliers to obtain a reliable image, which should have similar features to the model obtained by the robust inversion.

Nyamandhlovu area, Zimbabwe

Figures 9 and 10 show another example of investigating the effect of the potential errors on the inverted models. Figure 9 shows the inverted models of the robust inversion with different potential error levels for the Zimbabwe site. The potential error magnitude and the distribution of the outliers were shown in Fig. 5. From these results, it can be seen that even though the mean value (ε=11.8%) and standard deviation (σ=32.3%) of the potential errors were relative large, the four inverted models are quite stable in most parts of the line. The section from x=0 m to about x=600 m has a relatively low resistivity base-

ment starting from the depth of 20 m to 80 m, but in the neighbouring section from x=800 m to x=1600 m there appears a reverse structure (a low-resistivity top layer with a high-resistance basement). These two parts exhibit no serious effect from the outliers shown in Fig. 5b. In particular, the section from x=1100 m to x=1500 m consistently shows the high-resistance basement, although the number of data points changes from 661 in the original data set to 287 for the lowest error level. The big change in data density in this section still yielded a stable image with the robust inversion. It definitely proves insensitivity of the inversion to both the outliers and data density. However, the section from x=1750 m to the end of line (x=2200 m) did not survive either the data outliers or the loss of data density. The thin high-resistance top layer (over 1000 Ωm) that starts at x=1300 m is obvious and is caused by the Kalahari sand, but the presence of the high-resistance basement appears unreliable because of the inconsistent images with the decrease in the error levels in the inverted models (see dash-lined zone in Fig. 9). This inconsistency of the images may relate to the reduction in data density (the number of data points in this part was reduced from 664 in the original data set to 256 for the last error level) in combination with insufficient coverage of data points (known as the 'edge effect'), or the effect of the outliers in this part (see the same part in Fig. 5b). However, the appearance of so many outliers in this part gives a warning of bad conditions for the imaging surveying, e.g. high electrode contact resistance due to the highly resistant thin top layer.

Figure 10 shows the inverted models from the smoothness-constrained least-squares inversion with different potential error levels for the Zimbabwe site. Comparing the inverted model in Fig. 10a with the others (Fig. 10b, c and d), the difference in the images between the two sections can be seen (see dash-lined zones in Fig. 10): from x=1000 m to x=1300 m and from x=1700 m to the end of the line (x=2200 m). In Fig. 10a, a conductive vertical narrow 'dyke' appeared between x=1000 m and x=1200 m, but in the others it seems to disappear. With the decrease in the potential error levels, two buried high resistivity 'bodies' between the section 1700 m and 2200 m in Fig. 10a merge together and their resistivity values are changed from over 1000 Ωm to about 500 Ωm. Obviously, these two visible differences are related to the distribution of the outliers in the two sections (see Fig. 6). Viewing Figs 9d and 10d, it can be seen that they are very similar except that the former has a more 'blocky' appearance. These results, once again, show that the smoothness-constrained least-squares inversion is more sensitive to the outliers than the robust inversion and the two inversion schemes may produce quite similar images with high data quality. In other words, if the normal measurement does not contain serious outliers these two inversions may give similar structures for a resistivity imaging survey. The only difference is that the robust inversion produces a more 'blocky' structure and a slightly better data misfit than the smoothness-constrained least-squares inversion. From the final image, Fig. 9d or Fig. 10d, we appear to obtain a reliable picture of the resistivity structure: from x=0 m to x=800 m, a layer of higher resistivity is covering a low-resistivity layer. Several outcrops of basalt were found along this part, which indicates that this high-resistivity top layer is most likely basalt. The low-resistivity layer is probably the upper forest sandstone, according to available geological information. The section between x=800 m to x=1600 m implies a down-faulted block of basalt, caused by tectonic movement. This down-faulted block perhaps created a smaller basin where aeolian sands were deposited, which later formed ferricrete. Observation of a significant ridge of ferricrete in this part and the very low resistivity which may be due to the iron content strengthens this assumption. The very high resistivity thin layer starting from x=1350 m to the end of the line (x=2200 m) is the Kalahari sand.

CONCLUSIONS

We have analytically evaluated the magnitudes, illustrated the possible spreading patterns and numerically investigated the possible effects on imaging of the in-line and off-line spacing errors, which may occur in 2D resistivity imaging surveys. The results show that the off-line spacing error is much smaller than the in-line spacing error, and that the magnitudes of errors in measured data due to spacing errors depend on different electrode configurations. For example, 10% in-line spacing errors may have over 20% effect on the values for dipole-dipole, Wenner-β and γ-array data, whereas the other electrode arrays give smaller errors. The different electrode arrays in 2D resistivity imaging survey have different spreading patterns of the error effect, which radiate from erroneous electrodes with the magnitude decreasing with increased electrode spacing. Artefacts, close to the erroneous electrodes, appear in the inverted models due to in-line spacing errors, especially with dipole-dipole, Wenner-β and γ-array surveys. Similar artefacts or distorted images also may occur due to the small fixed 3D variations near the electrodes.

The data quality, or the observed potential error, may be estimated by normal and reciprocal measurements. Such data can be acquired efficiently using an automatic data acquisition system for all data points, although at the cost of increased surveying time. Our experiences show that the visualization alogarithmic plot and the error pseudosection of the absolute relative errors calculated by the normal and reciprocal potential readings are very useful for quantitative and spatial evaluation of the data quality, which may be characterized by the mean value, standard deviation, regres-

sion function and the spatial distribution of the possible observed outliers. The visualization may directly reflect the working status of the instrument, electrode contact resistant problems, background noise of the site and perturbing sources of the potential outliers in an imaging measurement. Our analysis of the potential errors for different sites and different electrode configurations shows that the potential error increases as a power with the decrease in the measured potential, which reaffirms the fact that the potential error depends on the strength of the measured signal and varies with sites, times and electrode configurations. The potential signal strength depends on electrode arrays and practical geological models. Generally speaking, Wenner, pole-pole and Schlumberger measurements have relative stronger potential signal than dipole-dipole and pole-dipole arrays. This may be simply proved by comparison of the inverse geometric factor of the electrode arrays.

We also show that the robust inversion and smoothness-constrained least squares inversion can be applied to the assessment of real observed potential outliers and data quality of the normal surveying data. The examples given in this paper show that the smoothness-constrained least-squares inversion is sensitive to outliers in the data, which may produce artifacts or distorted images in the inverted model. The examples also show that that artifacts or distorted images correlate with the distribution zones of the outliers in the error pseudosection. The robust inversion is fairly insensitive to the outliers of data, and with high data quality, i.e. all the potential errors obtained by normal and reciprocal measurements are less than 5%, the two inversion schemes produce very similar images except that that obtained with the robust inversion is more 'blocky' and has a slightly better data misfit. The common features of the inverted models from the two inversion schemes and the sections having high data quality can be expected to give a reliable image of the site.

ACKNOWLEDGEMENTS

The work presented here was supported by research grants from Elforsk, Svenska Kraftnät, DSIG (Dam Safety Interest Group), the Wenner-Gren Foundation, the Swedish Institute and Carl Trygger's Foundation, which is gratefully acknowledged. Furthermore, the work in Zimbabwe was funded by Sida/SAREC, and the Swedish Railway Administration funded the work carried out at Åkarp.

REFERENCES

Andersson S. and Engman, M. 2000. *Geophysical investigations of Karoo aquifers in the Nyamandhlovu area, Zimbabwe*. MSc thesis, Lund University.

Chambers J., Ogilvy R., Meldrum P. and Nissen J. 1999. 3D resistivity imaging of buried oil-and tar-contaminated waste deposits. *European Journal of Environmental and Engineering Geophysics* **4**, 117–128.

Claerbout J.F. and Muir F. 1973. Robust modelling with erratic data. *Geophysics* **38**, 826–844.

Constable S.C., Parker R.L. and Constable C.G. 1987. Occam's inversion: A practical algorithm for generating smooth models from electromagnetic sounding data. *Geophysics* **52**, 289–300.

Dahlin T. 1993. *On the automation of 2D resistivity surveying for engineering and environmental applications*. PhD thesis, Lund University.

Dahlin T. 1996. 2D resistivity surveying for environmental and engineering applications. *First Break* 14, 275–283.

DeGroot-Hedlin C. and Constable S. 1990. Occam's inversion to generate smooth, two-dimensional models from magnetotelluric data. *Geophysics* **38**, 826–844.

Ellis R.G. and Oldenburg D.W. 1994. Applied geophysical inversion. *Geophysical Journal International* **116,** 5–11.

Johansson S., Friborg J. and Dahlin T. 2000. *New and improved monitoring systems for embankment dams*. Elforsk report: 00:14.

Kennett B.L.N. and Williamson P.R. 1988. Subspace methods for large-scale non-linear inversion. In: *Mathematical Geophysics, a Survey of Recent Developments in Seismology and Geodynamics* (eds N.J. Vlaar, G. Nolet, M.J.R. Wortel and S.A.L. Cloetingh), pp. 139–154. D. Reidel, Dordrecht.

LaBrecque D., Miletto M., Daily W., Ramirez A. and Owen E. 1996. The effects of "Occam" inversion of resistivity tomography data. *Geophysics* **61**, 538–548.

Madsen K. and Nielsen H.B. 1993. A finite smoothing algorithm for linear L1 estimation. *SIAM Journal of Optimisation* **3**(2), 223–235.

Olayinka A. and Yaramanci U. 1999. Choice of the best model in 2-D geoelectrical imaging: case study from a waste dump site. *European Journal of Environmental and Engineering Geophysics* **3**, 221–244.

Oldenburg D.W., McGillicray P.R. and Ellis R.G. 1993. Generalised subspace methods for large-scale inverse problems. *Geophysical Journal International* **114**, 12–20.

Oldenburg D.W. and Yaoguo Li 1994. Inversion of induced polarization data. *Geophysics* **59**, 1327–1341.

Park S.K. and Van G.P. 1991. Inversion of pole-pole data for 3-D resistivity structure beneath arrays of electrodes. *Geophysics* **56**, 951–960.

Sasaki Y. 1992. Resolution of resistivity tomography inferred from numerical simulation. *Geophysical Prospecting* **40**, 453–464.

Skilling J. and Bryan R.K. 1984. Maximum entropy image reconstruction, general algorithm. *Mon. Not. R. ast. Soc*., **211**, 111–124.

Van G.P., Park S.K. and Hamilton P. 1991. Monitoring leaks from storage ponds using resistivity methods. *Geophysics* **56**, 1267–1270.

Wolke R. and Schwetlick H. 1988. Iteratively reweighted least squares: algorithms, convergence analysis, and numerical comparisons. *SIAM Journal of Scientific Statistics and Computing* **9,** 907–921.